

DeepMLE: A Robust Deep Maximum Likelihood Estimator for Two-view Structure from Motion

Yuxi Xiao, Li Li, Xiaodi Li and Jian Yao*

Abstract—Two-view structure from motion (SfM) is the cornerstone of 3D reconstruction and visual SLAM (vSLAM). Many existing end-to-end learning-based methods usually formulate it as a brute regression problem. However, the inadequate utilization of traditional geometry model makes the model not robust in unseen environments. To improve the generalization capability and robustness of end-to-end two-view SfM network, we formulate the two-view SfM problem as a maximum likelihood estimation (MLE) and solve it with the proposed framework, denoted as DeepMLE. First, we propose to take the deep multi-scale correlation maps to depict the visual similarities of 2D image matches decided by ego-motion. In addition, in order to increase the robustness of our framework, we formulate the likelihood function of the correlations of 2D image matches as a Gaussian and Uniform mixture distribution which takes the uncertainty caused by illumination changes, image noise and moving objects into account. Meanwhile, an uncertainty prediction module is presented to predict the pixel-wise distribution parameters. Finally, we iteratively refine the depth and relative camera pose using the gradient-like information to maximize the likelihood function of the correlations. Extensive experimental results on several datasets prove that our method significantly outperforms the state-of-the-art end-to-end two-view SfM approaches in accuracy and generalization capability.

I. INTRODUCTION

Two-view structure from motion (SfM) aims to recover the 3D structure (depth map) and motion (relative camera pose) from two consecutive images. As the cornerstone of 3D reconstruction and visual simultaneous localization and mapping (vSLAM), this fundamental techniques is widely applied in high-level tasks like autonomous driving [1], augmented/virtual reality [2], and robotics [3], [4].

Traditional SfM methods usually follow the pipeline of features extraction [5], sparse 2D image matching [6], relative camera pose computation [7], [8], [9] and 3D triangulation [10]. The dense depth map is hard to attain in this pipeline due to the sparsity of 2D image matches. Therefore, the direct methods have been proposed [11], [12], which simultaneously calculate a semi-dense depth map and relative camera pose by minimizing the photometric residuals between two images. However, whatever the feature-based or the direct methods are hard to remain robust in the lighting variable condition and dynamic environments [13].

To overcome these problems, many deep learning-based two-view SfM methods have been proposed recently. In general, learning-based methods can be divided into two categories. The first class [14], [15], [16] focuses on explicitly learning to match, and the calculation for the depth

map and the relative camera pose is left to traditional algorithms [10]. The second one tends to generate a dense monocular depth map and relative camera pose using an end-to-end network [17], [18], [19], [20], [21]. Compared to the first class, the latter benefits from the end-to-end training and inference, and it is usually more efficient. However, developing a robust and generalizable, end-to-end two-view SfM framework remains a challenging task [22]. Therefore, in this paper, we focus on the discussion of the end-to-end learning-based two-view SfM methods.

To improve the generalization capability and robustness of end-to-end two-view SfM networks, we propose to integrate maximum likelihood estimation (MLE) into our designed architecture. First, we propose to learn the multi-scale correlation volumes as a fine depiction for the correspondence of pixels. Then, we formulate the likelihood function of correlations of 2D image matches as a Gaussian and Uniform mixture distribution, and an uncertainty module is designed to predict the parameters of the distribution for each pixel. In this mixture distribution, tiny visual differences or illumination changes can be approximated by the Gaussian distribution, while the outliers of observations caused by extreme illumination change, oclusions and moving objects can be modeled by the Uniform distribution. Last, we solve this MLE problem by a proposed deep network instead of using traditional methods. The proposed deep network iteratively searches the optimal depth map and relative camera pose by maximizing the likelihood of observations. Thus, we do not need to manually design the regularizers or priors. Our model can implicitly learn these information from labeled data. The main contributions of our work can be summarized as:

- We propose to integrate the MLE into the DNNs to maximize the likelihood of correlations of 2D image matches, where the likelihood function is modeled as the Gaussian and Uniform mixture distribution.
- We design an end-to-end DNN to iteratively search the optimal estimation to maximize the likelihood using the gradient-like information, which solves the proposed MLE problem efficiently.
- The proposed DeepMLE achieves state-of-the-art performance and significantly outperforms existing end-to-end two-view SfM methods in both accuracy and generalization capability.

II. RELATED WORKS

A. Traditional Two-view SfM

Traditional methods commonly recover a sparse monocular depth map and relative camera pose by a set of 2D image

*Corresponding Author.

The authors are with the School of School of Remote Sensing and Information Engineering, Wuhan University, Wuhan, Hubei, P.R. China.

matched points. Thus, the key of traditional methods is 2D images points matching. To this end, a lot of hand-crafted and distinctive descriptors (e.g. SIFT [23], ORB [6], SURF [5]) were proposed to find the 2D image matches. Although these descriptors are enabled to attain accurate 2D image matches for keypoints, it is impractical to calculate dense 2D image matches for the limitations of computational cost and time [6], [24]. To reduce the computational cost and generate the semi-dense depth map, DSO [11] and LSD[12] employed photometric bundle adjustment to recover the semi-dense depth map and relative camera pose simultaneously. In addition, in order to alleviate the influence of photometric noise, DTAM [25] proposed to minimize the photometric residuals along with a TV-L1 regularization. However, the photometric residuals may fail in the conditions of illumination changes and less texture.

B. Learning-based Two-view SfM

Generally, existing learning-based methods can be divided into two types [22] including **Partial Learning methods** and **Whole Learning methods**. **Partial Learning methods** leverage the powerful representation ability of DNNs to explicitly learn to match, and the most of rest calculations are finished by classic geometry methods. **Whole Learning methods** pursue to develop a robust pipeline that is end-to-end during the training and the inference.

Partial Learning methods. These methods use the DNNs to extract deep features and explicitly learn the correspondences of pixels. Such correspondences can be represented as the explicit matches, featuremetric loss or the optical flow. Recent works [26], [16], [27] proposed to apply the deep optical flow network to find the 2D image matches, the relative camera pose can be directly calculated from the matched points using classical algorithms [8], [9]. After that, an extra depth estimation module is applied in their framework to further regress the depth map. Specially, Wang *et al.* [26] proposed a scale-invariant depth module to recover the depth map. In their module, the scale of predicted relative camera pose is applied to guide the estimation of the depth map. However, the works above can only estimate the relative camera pose and the depth with two separate stages. Simulating the traditional direct methods, BA-Net [21] applied a DNN to extract dense and distinctive visual features to define the featuremetric loss, and then simultaneously estimated a monocular depth map and relative camera pose via bundle adjustment.

Whole Learning methods. These methods attempt to find an end-to-end mapping from two-view images to original 3D structure and motion. In general, these methods can be categorized as self-supervised and supervised methods. The self-supervised methods [20], [28], [19], [19] usually apply the photometric residuals to train the DNNs. In general, they simply apply the U-Net-like convolutional network [29] to directly regress the depth map and relative camera pose. However, the photo-consistency assumption, which assumes the photometric residuals of two matched points should be

small, may be violated by the illumination changes and inherent image noise. In addition, it is difficult to minimize the photometric residuals if the intensity gradient is low and the texture information is poor. Yang *et al.* [30] estimated the affine brightness transformation for two images and photometric uncertainty for each pixel to alleviate the influence of illumination changes. For supervised methods, the ground truth is applied to train the network. LS-Net [17] applied the LSTM-RNN as an optimizer to minimize the photometric residuals iteratively, and they took the Jacobian matrix computed by Tensorflow as the input to regress the update of the depth map and relative camera pose. But the Jacobian matrix calculation is memory and time consuming. DeMoN [31] proposed a coarse-to-fine architecture and alternately refined the optical flow, depth and motion. DeepSFM [18] proposed to iteratively and alternately refine the initial depth map and initial relative camera pose offered by DeMoN [31]. Differently, our DeepMLE does not require the initial depth or relative camera pose, and meanwhile, our method is beneficial from MLE-based inference which clearly show the likelihood probabilistic of estimations.

III. METHOD

In this section, we are going to introduce how the MLE inference is integrated into the networks. To this end, the general maximum likelihood formula is introduced in Section III-A firstly, which demonstrates the process of MLE modelling as a whole. Subsequently, our DeepMLE is introduced to implement the MLE model by three sub-modules in Section III-B. The overview of DeepMLE is shown in Fig. 1.

A. Maximum Likelihood Formula for Two-view SfM

In the two-view SfM problem, given two consecutive images, the target image I_t and the source image I_s , the depth map \mathbf{D} of I_t and relative camera pose \mathbf{T} from I_t to I_s can be estimated by maximizing the likelihood of the correlations. In traditional methods, minimizing the photometric residuals also provide a maximum likelihood solution for the depth and relative camera pose estimation [11], [12]. In order to increase the robustness of the observations, we take the pixel-wise deep correlations as the observations for estimation $(\hat{\mathbf{D}}, \hat{\mathbf{T}})$. Meanwhile, we use $C(I_t, I_s)$ (see Section III-B.1) to denote the domain of deep correlation observations, which stores the all-pair correlation values in the target image I_t and the source image I_s . For each pixel-wise observation c , its value can be looked-up in $C(I_t, I_s)$. The aim of our work is to find the optimal depth map \mathbf{D} and relative camera pose \mathbf{T} that can maximize the likelihood of observations. The definition is formulated as:

$$\{\mathbf{D}, \mathbf{T}\} = \arg \max_{\hat{\mathbf{D}}, \hat{\mathbf{T}}} \prod_{i=1}^V P(c_i | \hat{\mathbf{D}}, \hat{\mathbf{T}}), \quad (1)$$

where V is the pixel number of the target image I_t . For each pixel in I_t , its correlation observation with its correspondence in I_s can be approximated by a Gaussian distribution when only relatively tiny illumination changes happen, but it more likely follow a Uniform distribution if the extreme illumination changes, occlusions and objects moving

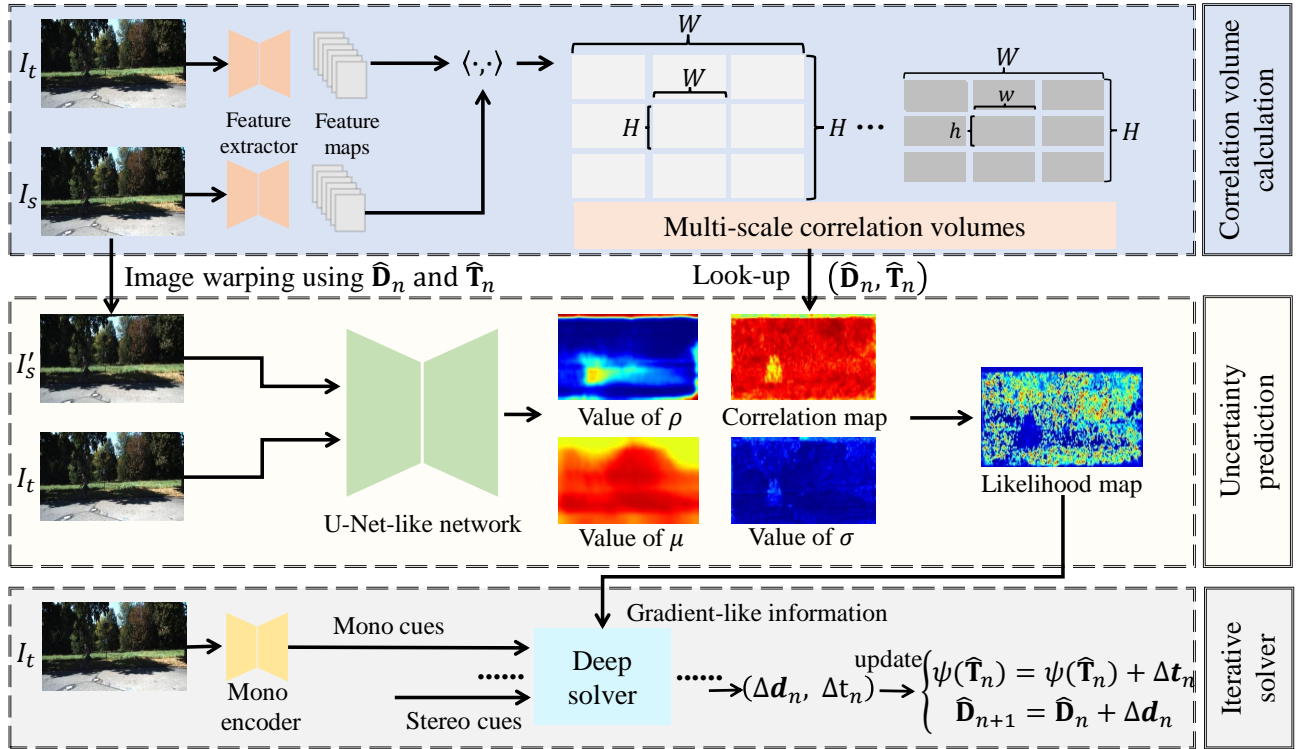


Fig. 1: The overview of the proposed DeepMLE. At every iteration, the observation of correlations are looked-up in correlation volumes. And then the uncertainty prediction module predicts the uncertainty parameters for every pixel. After attaining the correlation map and uncertainty parameters, the likelihood map and gradient information can be computed. Finally, the update of depth and pose are inferred by deep iterative solver with the input of gradient-like information.

appear. Therefore, we assume that the observations follow a Gaussian and Uniform mixture distribution. Thus, for each observation c_i , the likelihood can be calculated as:

$$P(c_i | \hat{\mathbf{D}}, \hat{\mathbf{T}}) = (1 - \rho_i) \mathcal{N}(c_i | \mu_i, \sigma_i) + \rho_i \mathcal{U}(c_i - 1, 1), \quad (2)$$

where μ_i and σ_i denote the mean and standard deviation, respectively, and ρ_i represents the weight between Gaussian and Uniform distributions (see Section III-B.2).

B. Architecture of DeepMLE

As shown in Fig. 1, our DeepMLE implements the MLE model discussed in Section III-A by three sub-modules: correlation volume calculation, uncertainty prediction and deep iterative solver.

1) *Correlation Volume Calculation*: As we know, the pixel correspondences between the target image I_t and the source image I_s are the bridge between 2D and 3D vision. However, both hand-crafted descriptors and photometric residuals have several inherent drawbacks which decrease the robustness of the algorithms.

Thus, to increase the robustness of the observations, we propose to apply a DNN to learn the representations for pixel-wise correlations. We firstly extract the dense deep features of the target image I_t and the source image I_s with a weight-shared extractor Φ_{corr} . And $\mathbf{F}_t, \mathbf{F}_s \in \mathbb{R}^{H \times W \times D}$ denote the deep features of I_t and I_s (the height H and width W of deep features are a quarter of those of I_t , and the channel number D is set to 256). Then, for every pixel in I_t , we dot product its normalized deep features

vector with the normalized features of every pixel in I_s . By this operation, we can construct a 4D correlation volume $\mathbf{V} \in \mathbb{R}^{H \times W \times H \times W}$ for all pairs in I_t and I_s .

In addition, to increase the receptive field, we downsample the last two dimension of \mathbf{V} to build a correlation pyramid $\{\mathbf{V}_k\}_{k=0}^2$, where \mathbf{V}_k has dimensions of $W \times H \times \frac{W}{2^k} \times \frac{H}{2^k}$. The correlation pyramid is the domain of observations, and it is denoted as $C(I_t, I_s)$. For each pixel $\mathbf{p} \in I_t$, the corresponding pixel position \mathbf{p}' in I_s can be calculated as:

$$\mathbf{p}' \sim \mathbf{K} \hat{\mathbf{T}} \hat{\mathbf{D}}(\mathbf{p}) \mathbf{K}^{-1} \mathbf{p}, \quad (3)$$

where \mathbf{K} is the intrinsic of camera, and $\hat{\mathbf{D}}(\mathbf{p})$ denote the depth of pixel \mathbf{p} , while $\hat{\mathbf{T}} = [\hat{\mathbf{R}} | \hat{\mathbf{t}}]$ is the transform matrix. $\hat{\mathbf{R}}$ is the relative rotation matrix and $\hat{\mathbf{t}}$ is the relative translation vector. Thus, for each pair $(\mathbf{p}, \mathbf{p}')$, we can directly look up the correlation value from $C(I_t, I_s)$ according to their positions. We can easily generate the correlation map $I_{\text{corr}} \in \mathbb{R}^{H \times W}$ and this correlation map I_{corr} is actually the observation for current estimations $(\hat{\mathbf{D}}, \hat{\mathbf{T}})$.

2) *Uncertainty Prediction*: For each pixel pair $(\mathbf{p}, \mathbf{p}')$, their correlation is influenced by illumination, occlusion or moving objects and image noise. Thus, we design an uncertainty prediction module to estimate the uncertainty parameters, $\{\rho_i, \mu_i, \sigma_i\}$ in Eq. (2), for each pixel. Here, we apply a U-Net-like network to predict the uncertainty parameters with the input of the target image I_t and the warped image I'_s of the source image I_s . Let Φ_{unc} denote the uncertainty network, the uncertainty parameters are estimated

as:

$$(I_\rho, I_\mu, I_\sigma) = \Phi_{\text{unc}}(I'_s, I_t). \quad (4)$$

It should be noted that we do not need the ground truth of uncertainty parameter maps to train the network. This module allows the network to adaptively predict the uncertainty using the input data, which improves the accuracy and robustness of the model.

After introduction of the uncertainty module, for any estimation $(\hat{\mathbf{D}}, \hat{\mathbf{T}})$, the corresponding likelihood map I_l can be directly calculated according to Eq. (2).

3) *Deep Iterative Solver*: For solving this MLE problem in an end-to-end way, we design a deep iterative solver which refines the depth and relative camera pose step by step. Inspired by the traditional gradient descent optimization algorithm, the proposed deep solver uses the gradient-like information of the depth map and relative camera pose to iteratively refine the initial estimation. Let Φ_{update} denote the network of deep iterative solver. Because the rotation matrix can not be updated by simple addition and subtraction, we first reparametrize the transform matrix $\hat{\mathbf{T}}_n$ to six parameters $\psi(\hat{\mathbf{T}}_n) = \{r_x, r_y, r_z, t_x, t_y, t_z\}$, which are the Lie Algebra for the transform matrix. Let $(\hat{\mathbf{D}}_n, \psi(\hat{\mathbf{T}}_n))$ denote the current estimation, we need to predict the update $(\Delta \mathbf{d}_n, \Delta \mathbf{t}_n)$ to generate the next estimation $(\hat{\mathbf{D}}_{n+1}, \psi(\hat{\mathbf{T}}_{n+1}))$,

$$\hat{\mathbf{D}}_{n+1} = \hat{\mathbf{D}}_n + \Delta \mathbf{d}_n, \psi(\hat{\mathbf{T}}_{n+1}) = \psi(\hat{\mathbf{T}}_n) + \Delta \mathbf{t}_n. \quad (5)$$

Gradient-like information. In order to mimic gradient descent method, we use difference approximation to obtain the first-order derivation of the depth and relative camera pose. For current estimation $(\hat{\mathbf{D}}_n, \psi(\hat{\mathbf{T}}_n))$, we give a set of fixed and tiny disturbance $\pm \Delta \mathbf{G} = (\Delta \hat{\mathbf{D}}_n, \Delta \psi(\hat{\mathbf{T}}_n))$ to slightly change the value of parameters. It should be noted that we give the same depth disturbance for all pixels to reduce the computational cost. After the disturbance, we can generate a set of new likelihood maps \mathcal{J}_l according to Eq. (2). Then, for $J_l^m \in \mathcal{J}_l$, the difference likelihood map $\Delta J_l^m = J_l^m - I_l$. The difference likelihood maps contain the gradient-like information for each parameter in $(\hat{\mathbf{D}}_n, \psi(\hat{\mathbf{T}}_n))$. So these difference likelihood maps are leveraged in next in update prediction.

Update prediction. We propose to use a gate recurrent unit (GRU) [32] to predict the update $(\Delta \mathbf{d}_n, \Delta \mathbf{t}_n)$. As shown in Fig. 2, the input of GRU includes three parts: the mono cues, the stereo cues and the output of last unit. The mono cues are extracted from the target image I_t using a CNN as the supplementary information for assisting the depth estimation especially in the areas of mutual invisibility. The stereo cues are extracted in the similar way presented in RAFT [33]. The output of GRU contains the temporal information of optimization. Then, we concatenate the output feature of GRU with the gradient-like information to predict the optimal gradient descent direction for parameter update using a CNN. After that, we directly obtain the transform matrix $\hat{\mathbf{T}}_{n+1} = \psi^{-1}(r_x, r_y, r_z, t_x, t_y, t_z)$. By this design, our update prediction module can leverage not only the

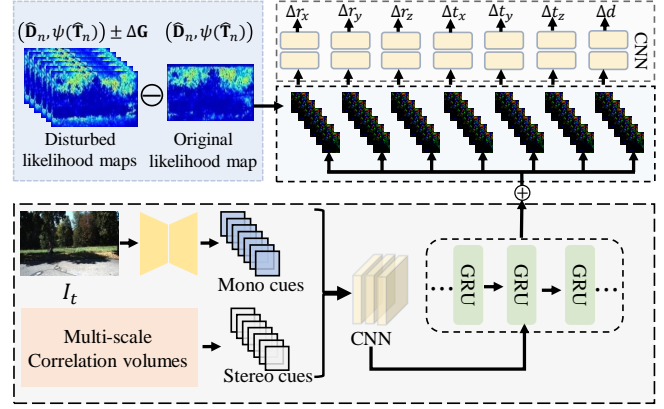


Fig. 2: The architecture of our proposed deep iterative solver. Disturbed likelihood maps are computed by a set of disturbed depth and relative camera pose. The update of \mathbf{G} (depth and relative camera pose) are predicted by seven different CNN heads with the input of difference likelihood map and GRU output.

temporal and also the spatial information of the optimization to give a more accurate prediction.

C. Loss Function

Our whole model contains three sub-modules, namely, $\Phi_{\text{corr}}, \Phi_{\text{unc}}, \Phi_{\text{update}}$. Let $\theta_{\text{corr}}, \theta_{\text{unc}}$ and θ_{update} denote the model parameters of these three sub-modules, respectively. The most widely used loss is the L_2 norm [18], [34], [31] between prediction $(\hat{\mathbf{D}}_n, \hat{\mathbf{T}}_n)$ and ground truth $(\mathbf{D}_{gt}, \mathbf{T}_{gt})$, this regression loss \mathcal{L}_{reg} is defined as:

$$\mathcal{L}_{\text{reg}} = \sum_{n=1}^N (\|\alpha_n \hat{\mathbf{D}}_n - \mathbf{D}_{gt}\|_2 + \|\hat{\mathbf{R}}_n - \mathbf{R}_{gt}\|_2 + \|\alpha_n \hat{\mathbf{t}}_n - \mathbf{t}_{gt}\|_2), \quad (6)$$

where N is the number of iterations and α_n is the scale factor between ground truth and current estimation. However, just using \mathcal{L}_{reg} can not give adequate and clear constrains for three sub-modules. To give more specific and proper supervision signals for each module, we further propose a probabilistic loss $\mathcal{L}_{\text{prob}}$ and a likelihood increase loss \mathcal{L}_{inc} .

Probabilistic loss. This loss is designed to find the optimal estimation of θ_{corr} and θ_{unc} . We also use the maximum likelihood estimation to estimate θ_{corr} and θ_{unc} as follows:

$$\begin{aligned} \{\theta_{\text{corr}}, \theta_{\text{unc}}\} &= \arg \max_{\hat{\theta}_{\text{corr}}, \hat{\theta}_{\text{unc}}} P(I_{\text{corr}} | \hat{\theta}_{\text{corr}}, \hat{\theta}_{\text{unc}}), \\ P(c | \hat{\theta}_{\text{corr}}, \hat{\theta}_{\text{unc}}) &= \sum_{n=1}^N \left(\prod_{c \in I_{\text{corr}}} P(c | \hat{\mathbf{D}}_n, \hat{\mathbf{T}}_n, \hat{\theta}_{\text{corr}}, \hat{\theta}_{\text{unc}}) P(\hat{\mathbf{D}}_n, \hat{\mathbf{T}}_n | \mathbf{D}_{gt}, \mathbf{T}_{gt}) \right) \end{aligned} \quad (7)$$

We assume that the $P(\hat{\mathbf{D}}_n, \hat{\mathbf{T}}_n | \mathbf{D}_{gt}, \mathbf{T}_{gt})$ is a impulse-like distribution. The expression above can be converted into a probabilistic loss,

$$\begin{aligned} \mathcal{L}_{\text{prob}} &= - \sum_{n=1}^N e^{l_n - \frac{\mathcal{L}_{\text{reg}}^n}{\sigma}}, \\ l_n &= \frac{\sum_{c \in I_{\text{corr}}} \log(P(c | \hat{\mathbf{D}}_n, \hat{\mathbf{T}}_n, \hat{\theta}_{\text{corr}}, \hat{\theta}_{\text{unc}}))}{V}, \end{aligned} \quad (8)$$

where σ is a hyper-parameter for the impulse-like distribution, and $\mathcal{L}_{\text{reg}}^n$ is the regression loss of the n -th iteration. l_n denotes the average likelihood of current observations.

Likelihood increase loss. In order to give a clear and specific supervision signal to estimate θ_{update} , we design a

likelihood increase loss \mathcal{L}_{inc} . In this loss, we expect that the likelihood of current iteration can rapidly increase when the different between current estimation and ground truth is large. Otherwise, the likelihood tends to convergence. \mathcal{L}_{inc} is defined as:

$$\mathcal{L}_{\text{inc}} = \sum_{n=1}^N (l_n - l_{n+1}) \log(1 + \mathcal{L}_{\text{reg}}^n). \quad (9)$$

Finally, our total loss can be expressed as below,

$$\mathcal{L}_{\text{total}} = \alpha_1 \mathcal{L}_{\text{reg}} + \alpha_2 \mathcal{L}_{\text{inc}} + \alpha_3 \mathcal{L}_{\text{prob}}, \quad (10)$$

where α_1 , α_2 and α_3 are three hyper-parameters.

IV. EXPERIMENTS

In this section, we first introduce the implementation details of our network. Then, we present the evaluation results of our DeepMLE in both accuracy and generalization. Meanwhile, we carefully compare our DeepMLE with the state-of-art **Partial Learning methods** and **Whole Learning methods** (Seen in SectionII-B). And in this section, we denote these two types methods as **Type I** and **Type II** methods, respectively. Finally, we give the ablation study to justify our design for each module.

A. Implementation Details

We implemented our framework using PyTorch. For the training on the KITTI dataset [35], we trained our model on one NVIDIA RTX 3090 GPU to convergence on all 40k training two-view pairs. In order to accelerate the training, we first initialized our model by training it with low resolution images (188×620). And in initialization, we set the α_1 , α_2 , and α_3 in the total loss as shown in Eq. (10) to 0.05, 1, 0.05, respectively. After initialization training, we refined our model with high resolution images (256×832). And α_1 , α_2 , and α_3 was set to 1, 1, and 1, respectively. The number of iterations was set to 8. The total time of training costs 10 days for six epochs. The initialization training was done with a batch size of 2 and a learning rate of 5×10^{-4} in first two epochs. And the last four epochs are in the refining procedure with a batch size of 1 and a learning rate of 8×10^{-5} . The training optimizer is AdamW [36], and the gradients were clipped into $[-1, 1]$. For the training in DeMoN [31], the learning rate was set to 5×10^{-5} in the first eight epochs and the α_1 , α_2 , and α_3 were set to 0.5, 2, and 1, respectively, and in the last four epochs the learning rate was set to 5×10^{-6} . The number of iterations was also set to 8.

B. Datasets

KITTI. KITTI is a widely used benchmark dataset in automatic driving tasks. For depth evaluation, we conducted the experiments on Eigen split [37]. In order to adapt it for evaluating the depth estimation for SfM, we additionally selected the near image of the target image as the source image, which is the same scheme applied in [26]. For pose evaluation, we followed the most popular evaluation fashion in end-to-end SfM methods [19], [20], [26] to train our model in the first 8 sequences in KITTI odometry and test it in the ‘‘09’’ and ‘‘10’’ sequences.

vKITTI. vKITTI [38] contains several sequences of virtual data including different imaging and weather conditions. In order to evaluate the generalization capability of our network, we follow the setting in the domain-adaptation task[39]. We trained DeepMLE in vKITTI and evaluated the depth estimation in KITTI without any fine-tune.

DeMoN dataset. DeMoN dataset [31] selects the data from various sources including SUN3D [40], RGB-D [41] and Scenes11 [42]. It contains both indoor and outdoor scenes. Therefore, this comprehensive dataset is representative in evaluating the performance of the SfM pipeline. And for a fair comparison, we evaluated our methods with DeMoN metrics. Meanwhile, for further illusion of generalization capability of our work, we also tested DeepMLE on MVS dataset [43] which do not appear in our training data.

C. Accuracy Evaluation

KITTI. To evaluate the accuracy of the estimations of our method, our DeepMLE was tested on the KITTI for the separate evaluation of the estimation of the depth and the relative camera pose.

For the depth evaluation, we applied the metrics presented in [44] for fair comparison. Firstly, the qualitative results are presented in Fig. 3. The qualitative results clearly show that compared with the state-of-the-art approach, our DeepMLE performs more robustly in the scenes full of the dynamic objects, and these results owe to the proposed MLE inference. Secondly, the quantitative results are reported in Table I. Our DeepMLE has achieved a marked increase for two-view SfM framework. Compared to DeepV2D, which uses a sequence of frames including two closest frames before and after the target frame for training and inferring, our method only takes two consecutive image as input. But our method outperforms DeepV2D by a clear margin. The marked accuracy improvement proves the significance of the effective integration of MLE inference to our model. Meanwhile, compared to Wang *et al.* [26], the state-of-the-art **Type I** algorithm, our DeepMLE has achieved competitive results and have outperformed it in four metrics clearly. And in [26], the depth is estimated by an isolated module which is supervised by depth ground truth directly, which is more easy to fit ground truth in one data.

As the quantitative results shown in Table II, our method make a obvious progress for **Type II** two-view SfM method. Actually, learning to estimate relative camera pose directly by a neural network is much more challenging than estimating it by robust geometry algorithms. But our pipeline increases the accuracy of **Type II** methods by an order of magnitude. And our method achieves the competitive results with the ORB-SLAM2 with loop closure and back-end optimization. We visualized the trajectories of ‘‘09’’ and ‘‘10’’ sequences generated by different methods in Fig.4.

DeMoN dataset. We further conducted the experiments on DeMoN dataset, which contains comprehensive scenes of outdoor and indoor. For comparison, we directly borrow the results from the corresponding articles [18], [26]. Both traditional [49] and learning-based methods [21], [18], [34],



Fig. 3: The depth maps generated by the proposed DeepMLE and Wang *et al.* on KITTI dataset. These four scenes above include a lot of dynamic objects. The green boxes are applied to highlight the areas where depth are more accurately estimated by our DeepMLE.

TABLE I: Depth evaluation on KITTI dataset. The S and SS are short for ‘‘Supervised’’ and ‘‘Self-Supervised’’ respectively.

Split	Types	Methods	Lower is better				Higher is better		
			Abs Rel	Sq Rel	RMSE	RMSE _{log}	$\delta < 1.25$	$\delta < 1.25^2$	$\delta < 1.25^3$
Eigen	Type I	BA-Net [21]	0.083	-	3.640	0.134	-	-	-
		DeepV2D [34]	0.064	0.350	2.946	0.120	0.946	0.982	0.991
		Wang et al.[26]	0.055	0.224	2.273	0.091	0.956	0.984	0.993
	Type II (SS)	SfMLearner [19]	0.208	1.768	6.856	0.283	0.678	0.885	0.957
		monodepth2 [20]	0.115	0.903	4.863	0.193	0.877	0.959	0.981
		GLNet [45]	0.099	0.796	4.743	0.186	0.884	0.955	0.979
		D3VO[30]	-	-	4.485	0.185	0.885	0.958	0.979
	Type II (S)	DeepMLE (Ours w/o uncertainty)	0.065	0.212	2.628	0.095	0.955	0.984	0.994
		DeepMLE (Ours w/o MLE)	0.091	0.367	3.257	0.129	0.920	0.985	0.996
		DeepMLE (Ours full)	0.060	0.203	0.257	0.089	0.967	0.995	0.999

TABLE II: Pose estimation accuracy on the KITTI VO dataset.

Methods	Seq. 09		Seq. 10	
	$t_{err}(\%)$	$r_{err}(\circ/100m)$	$t_{err}(\%)$	$r_{err}(\circ/100m)$
ORB-SLAM2 (wo/ LC) [24]	9.30	0.26	2.57	0.32
ORB-SLAM2 (w/ LC) [24]	2.88	0.25	3.30	0.30
SfMLearner [19]	8.28	3.07	12.20	2.96
DeepV2D [34]	8.71	3.70	12.81	8.30
LTMVO [46]	3.49	1.03	5.81	1.81
Zhao <i>et al.</i> [27]	6.81	0.72	4.39	1.05
TartanVO [47]	6.00	3.11	6.89	2.73
CCNet [48]	4.32	1.69	5.35	3.16
DeepMLE (Ours)	1.46	0.76	1.28	0.67

[26], [17] are selected for comparison. In this dataset, we tested all methods on SUN3D, RGB-D and Scenes11 respectively. The evaluation results are presented in Table III. Although DeepSfM utilized the initialized depth map and relative camera poses estimated by DeMoN network, Our DeepMLE does not need any initialization and beats it by a clear margin in RGB-D and SUN3D datasets and achieves the similar performance in the Scenes11 dataset.

D. Generalization Evaluation

vKITTI to KITTI. The same metrics are used for depth and pose evaluation in generalization experiment. And we followed the experiment settings of the task of domain-adaptation. The vKITTI dataset was taken as the source dataset, while the KITTI was regarded as the target. We trained our DeepMLE in vKITTI, and tested it in KITTI

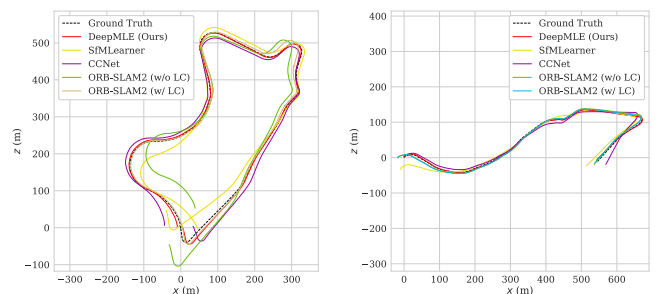


Fig. 4: The visualization of trajectory. Left: the visualization in sequence ‘‘09’’; Right: the visualization in sequence ‘‘10’’

without any fine-tune. As reported in Table IV, without any operation for domain adaptation, our DeepMLE outperforms the baseline by a clear margin and beats the state-of-the-art domain adaptation method [39] in six metrics. The results show that the introduction of MLE inference to deep neural network make the estimation more accurate.

MVS dataset. To further illustrate the generability ability of DeepMLE, we trained our method in SUN3D, Scenes11 and RGB-D and tested it in MVS dataset. It should be noted that the MVS dataset is very different to our training data. This dataset has been widely used for the generalization evaluation for SfM problem. As results shown in Table V, our DeepMLE beats DeepSfM [18], the state-of-the-art **Type II** SfM approach, by a clear margin, e.g., 0.014 versus 0.021

TABLE III: Results on DeMoN datasets. The traditional methods are reported in the first three rows. DeMoN, LS-Net and DeepSfM are the **Type II** methods. While Wang *et al.* [26] and BA-Net [21] are **Type I** methods.

Methods	RGB-D Dataset					Scenes11 Dataset					Sun3D Dataset				
	Depth			Pose		Depth			Pose		Depth			Pose	
	L1-inv	Sc-inv	L1-rel	Rot	Tran	L1-inv	Sc-inv	L1-rel	Rot	Tran	L1-inv	Sc-inv	L1-rel	Rot	Tran
Base-SIFT	0.050	0.577	0.703	12.010	56.021	0.051	0.900	1.027	6.179	56.650	0.029	0.290	0.286	7.702	41.825
Base-Matlab	-	-	-	12.813	49.612	-	-	-	0.917	14.639	-	-	-	5.920	32.298
COLMAP [49]	-	-	0.384	7.961	23.469	-	-	0.625	4.834	10.682	-	-	0.623	4.235	15.956
BA-Net [21]	0.008	0.087	0.050	2.459	14.900	0.080	0.210	0.130	3.499	10.370	0.015	0.110	0.060	1.729	13.260
Wang <i>et al.</i> [26]	-	-	-	-	-	0.005	0.097	0.058	0.276	2.041	0.010	0.081	0.057	1.391	10.757
DeMoN [31]	0.028	0.130	0.212	2.641	20.585	0.019	0.315	0.248	0.809	8.918	0.019	0.114	0.172	1.801	18.811
LS-Net [17]	0.019	0.090	0.301	1.010	22.100	0.010	0.410	0.210	4.653	8.210	0.015	0.189	0.650	1.521	14.347
DeepSfM [18]	0.011	0.071	0.126	1.862	14.570	0.007	0.112	0.064	0.403	5.828	0.013	0.093	0.072	1.704	13.107
DeepMLE (Ours)	0.005	0.065	0.068	2.067	13.893	0.005	0.126	0.079	0.386	3.764	0.007	0.091	0.068	1.261	9.763

TABLE IV: Generalization evaluation of depth estimation from vKITTI to KITTI. We compared our method with the state-of-the-art domain adaptation method S2R-DepthNet [39]. And we take a U-Net-like network as baseline which is trained by direct regression. Under the same hardware condition to us, we tested Wang *et al.* [26] method by their published codes.

Settings	Lower is better				Higher is better		
	Abs Rel	Squa Rel	RMSE	RMSE _{log}	$\delta < 1.25$	$\delta < 1.25^2$	$\delta < 1.25^3$
T ² Net[50] (vKITTI→KITTI)	0.171	1.351	5.944	0.247	0.757	0.918	0.969
S2R-DepthNet[39] (vKITTI→KITTI)	0.165	1.351	5.695	0.236	0.781	0.931	0.972
baseline (vKITTI→KITTI)	0.236	2.171	7.063	0.315	0.642	0.861	0.944
Kundu <i>et al.</i> [51](vKITTI→KITTI)	0.214	1.932	7.157	0.295	0.665	0.882	0.950
Wang <i>et al.</i> [26] (vKITTI→KITTI)	0.245	2.032	7.953	0.305	0.673	0.871	0.953
DeepMLE (Ours w/o uncertainty) (vKITTI→KITTI)	0.169	1.070	5.396	0.227	0.748	0.930	0.978
DeepMLE (Ours w/o MLE) (vKITTI→KITTI)	0.209	1.342	5.518	0.260	0.679	0.908	0.971
DeepMLE (Ours full) (vKITTI→KITTI)	0.164	1.005	5.135	0.218	0.773	0.939	0.980

TABLE V: Generalization evaluation on MVS dataset.

Method	MVS dataset				
	Depth			Pose	
	L1-inv	Sc-inv	L1-rel	Rot	Tran
Base-SIFT	0.056	0.309	0.361	21.180	60.516
Base-Matlab	-	-	-	10.843	32.736
COLMAP [49]	-	-	0.384	7.961	23.469
BA-Net [21]	0.030	0.150	0.080	3.499	11.238
Wang <i>et al.</i> [26]	0.015	0.102	0.068	2.417	3.878
DeMoN [31]	0.047	0.202	0.305	5.156	14.447
LS-Net [17]	0.051	0.221	0.311	4.653	11.221
DeepSfM [18]	0.021	0.129	0.079	2.824	9.881
DeepMLE (Ours)	0.014	0.103	0.072	1.261	9.762

in L1-inv and 0.103 versus 0.129 in Sc-inv.

E. Ablation Study

We conducted a set of experiments to justify the designs of each part of DeepMLE. The results of ablation studies are presented in the last three rows of Tables I and IV.

Uncertainty module. Taking no consideration of the uncertainty, we use the fixed parameters for the Gaussian and Uniform mixture distribution instead using the parameters predicted by proposed uncertainty module. The results presented in Tables I and IV shows that without the uncertainty module, the accuracy and generability capability of our network distinctly drop. These result further underlines the importance of the predictive uncertain parameters which alleviate the influence of illumination changes, occlusions and image noise.

MLE inference. In order to justify the significance of integrating the MLE inference into DNNs. We trained our framework by ablating the MLE inference parts, and the depth and relative camera pose are regressed from one block instead of iterative inference. And the results shown in

Tables I and IV, when the MLE inference is removed, the accuracy and generalization capability sharply drop in all the metrics. These two ablations experiments distinctly justify that the significance of the MLE inference for generalization capability and accuracy of our model.

V. CONCLUSIONS

In this paper, we creatively integrated the MLE inference into the designed deep neural network, which made the end-to-end model more interpretable and generalizable. Instead of using tradition methods to maximize the likelihood of the observations, we propose an end-to-end network to solve it using gradient-like information. Thus, we can take advantages of both learning-based method and traditional MLE method. Extensive experiments on several datasets illustrates that the proposed DeepMLE has achieved state-of-the-art performance in both generalization capability and accuracy.

VI. ACKNOWLEDGE

This work was partially supported by the National Natural Science Foundation of China (No. 42101440), the CCF-Baidu Open Fund (No.OF2021023), the Shenzhen Central Guiding the Local Science and Technology Development Program (No.2021Szvup100), and the LIESMARS Special Research Funding.

REFERENCES

- [1] A. Singandhupe and H. M. La, "A Review of SLAM Techniques and Security in Autonomous Driving," in *IEEE International Conference on Robotic Computing*, 2019.
- [2] Y. Yuan, Y. Ding, L. Zhao, and L. Lv, "An Improved Method of 3D Scene Reconstruction Based on SfM," in *International Conference on Robotics and Automation Engineering*, 2018.
- [3] R. Tiar, M. Lakrouf, and O. Azouaoui, "Fast ICP-SLAM for a Bi-steerable Mobile Robot in Large Environments," in *International Conference on Advanced Robotics (ICAR)*, 2015.

- [4] A. Merzlyakov and S. Macenski, "A Comparison of Modern General-Purpose Visual Slam Approaches," in *2021 IEEE/RSJ International Conference on Intelligent Robots and Systems (IROS)*. IEEE, 2021, pp. 9190–9197.
- [5] H. Bay, A. Ess, T. Tuytelaars, and L. Van Gool, "Speeded Up Robust Features (SURF)," *Computer Vision and Image Understanding*, vol. 110, no. 3, pp. 346–359, 2008.
- [6] E. Rublee, V. Rabaud, K. Konolige, and G. Bradski, "ORB: An Efficient Alternative to SIFT or SURF," in *International Conference on Computer Vision*, 2011.
- [7] M. Hu, K. McMenemy, S. Ferguson, G. Dodds, and B. Yuan, "Epipolar Geometry Estimation based on Evolutionary Agents," *Pattern Recognition*, vol. 41, no. 2, pp. 575–591, 2008.
- [8] H. Li and R. Hartley, "Five-Point Motion Estimation Made Easy," in *International Conference on Pattern Recognition*, 2006.
- [9] D. Nistér, "An Efficient Solution to the Five-Point Relative Pose Problem," *IEEE Transactions on Pattern Analysis and Machine Intelligence*, vol. 26, no. 6, pp. 756–770, 2004.
- [10] Andrew, Alex M., "Multiple view geometry in computer vision," *Kybernetes*, 2001.
- [11] J. Engel, V. Koltun, and D. Cremers, "Direct Sparse Odometry," *IEEE Transactions on Pattern Analysis and Machine Intelligence*, vol. 40, no. 3, pp. 611–625, 2017.
- [12] J. Engel, T. Schöps, and D. Cremers, "LSD-SLAM: Large-Scale Direct Monocular SLAM," in *European Conference on Computer Vision*, 2014.
- [13] A. Bhowmik, S. Gumhold, C. Rother, and E. Brachmann, "Reinforced Feature Points: Optimizing Feature Detection and Description for a High-Level Task," in *IEEE/CVF Conference on Computer Vision and Pattern Recognition*, 2020, pp. 4947–4956.
- [14] D. DeTone, T. Malisiewicz, and A. Rabinovich, "SuperPoint: Self-Supervised Interest Point Detection and Description," in *IEEE/CVF Conference on Computer Vision and Pattern Recognition Workshops*, 2018.
- [15] P.-E. Sarlin, D. DeTone, T. Malisiewicz, and A. Rabinovich, "SuperGlue: Learning Feature Matching With Graph Neural Networks," in *IEEE/CVF Conference on Computer Vision and Pattern Recognition*, 2020.
- [16] S. Li, X. Wu, Y. Cao, and H. Zha, "Generalizing to the Open World: Deep Visual Odometry with Online Adaptation," in *IEEE/CVF Conference on Computer Vision and Pattern Recognition*, 2021.
- [17] R. Clark, M. Bloesch, J. Czarnowski, S. Leutenegger, and A. J. Davison, "LS-Net: Learning to Solve Nonlinear Least Squares for Monocular Stereo," *arXiv preprint arXiv:1809.02966*, 2018.
- [18] X. Wei, Y. Zhang, Z. Li, Y. Fu, and X. Xue, "DeepSFM: Structure from Motion via Deep Bundle Adjustment," in *European Conference on Computer Vision*, 2020.
- [19] R. Mahjourian, M. Wicke, and A. Angelova, "Unsupervised Learning of Depth and Ego-Motion from Monocular Video Using 3D Geometric Constraints," in *IEEE/CVF Conference on Computer Vision and Pattern Recognition*, 2018.
- [20] C. Godard, O. M. Aodha, M. Firman, and G. Brostow, "Digging into Self-Supervised Monocular Depth Estimation," in *IEEE/CVF International Conference on Computer Vision*, 2019.
- [21] C. Tang and P. Tan, "BA-Net: Dense Bundle Adjustment Networks," in *International Conference on Learning Representations*, 2019.
- [22] H. Laga, L. V. Jospin, F. Boussaid, and M. Bennamoun, "A Survey on Deep Learning Techniques for Stereo-based Depth Estimation," *IEEE Transactions on Pattern Analysis and Machine Intelligence*, 2020.
- [23] D. G. Lowe, "Object Recognition from Local Scale-Invariant Features," in *IEEE International Conference on Computer Vision*, 1999.
- [24] R. Mur-Artal and J. D. Tardós, "ORB-SLAM2: An Open-Source SLAM System for Monocular, Stereo, and RGB-D Cameras," *IEEE Transactions on Robotics*, vol. 33, no. 5, pp. 1255–1262, 2017.
- [25] R. A. Newcombe, S. Izadi, O. Hilliges, D. Molyneaux, D. Kim, A. J. Davison, P. Kohli, J. Shotton, S. Hodges, and A. Fitzgibbon, "KinectFusion: Real-Time Dense Surface Mapping and Tracking," in *IEEE International Symposium on Mixed and Augmented Reality*, 2011.
- [26] J. Wang, Y. Zhong, Y. Dai, S. Birchfield, K. Zhang, N. Smolyanskiy, and H. Li, "Deep Two-View Structure-from-Motion Revisited," in *IEEE/CVF Conference on Computer Vision and Pattern Recognition*, 2021.
- [27] W. Zhao, S. Liu, Y. Shu, and Y.-J. Liu, "Towards Better Generalization: Joint Depth-Pose Learning Without PoseNet," in *IEEE/CVF Conference on Computer Vision and Pattern Recognition*, 2020.
- [28] J.-W. Bian, H. Zhan, N. Wang, Z. Li, L. Zhang, C. Shen, M.-M. Cheng, and I. Reid, "Unsupervised Scale-consistent Depth Learning from Video," *International Journal of Computer Vision*, vol. 129, p. 2548–2564, 2021.
- [29] O. Ronneberger, P. Fischer, and T. Brox, "U-Net: Convolutional Networks for Biomedical Image Segmentation," in *International Conference on Medical Image Computing and Computer-Assisted Intervention*, 2015, pp. 234–241.
- [30] N. Yang, L. von Stumberg, R. Wang, and D. Cremers, "D3VO: Deep Depth, Deep Pose and Deep Uncertainty for Monocular Visual Odometry," in *IEEE/CVF Conference on Computer Vision and Pattern Recognition*, 2020.
- [31] B. Ummerhofer, H. Zhou, J. Uhrig, N. Mayer, E. Ilg, A. Dosovitskiy, and T. Brox, "DeMoN: Depth and Motion Network for Learning Monocular Stereo," in *IEEE/CVF Conference on Computer Vision and Pattern Recognition*, 2017.
- [32] K. Cho, B. Van Merriënboer, D. Bahdanau, and Y. Bengio, "On the Properties of Neural Machine Translation: Encoder-Decoder Approaches," *arXiv preprint arXiv:1409.1259*, 2014.
- [33] Z. Teed and J. Deng, "RAFT: Recurrent All-Pairs Field Transforms for Optical Flow," in *European Conference on Computer Vision*, 2020, pp. 402–419.
- [34] Teed, Zachary and Deng, Jia, "DeepV2D: Video to Depth with Differentiable Structure from Motion," *arXiv preprint arXiv:1812.04605*, 2018.
- [35] A. Geiger, P. Lenz, and R. Urtasun, "Are We Ready for Autonomous Driving? The KITTI Vision Benchmark Suite," in *IEEE/CVF Conference on Computer Vision and Pattern Recognition*, 2012.
- [36] I. Loshchilov and F. Hutter, "Decoupled Weight Decay Regularization," *arXiv preprint arXiv:1711.05101*, 2019.
- [37] D. Eigen and R. Fergus, "Predicting Depth, Surface Normals and Semantic Labels with a Common Multi-Scale Convolutional Architecture," in *IEEE International Conference on Computer Vision*, 2015.
- [38] A. Gaidon, Q. Wang, Y. Cabon, and E. Vig, "VirtualWorlds as Proxy for Multi-Object Tracking Analysis," in *IEEE/CVF Conference on Computer Vision and Pattern Recognition*, 2016.
- [39] X. Chen, Y. Wang, X. Chen, and W. Zeng, "S2R-DepthNet: Learning a Generalizable Depth-specific Structural Representation," in *IEEE/CVF Conference on Computer Vision and Pattern Recognition*, 2021.
- [40] J. Xiao, A. Owens, and A. Torralba, "SUN3D: A Database of Big Spaces Reconstructed using SFM and Object Labels," in *IEEE International Conference on Computer Vision*, 2013.
- [41] J. Sturm, N. Engelhard, F. Endres, W. Burgard, and D. Cremers, "A Benchmark for the Evaluation of RGB-D SLAM Systems," in *IEEE/RSJ International Conference on Intelligent Robots and Systems*, 2012.
- [42] A. X. Chang, T. Funkhouser, L. Guibas, P. Hanrahan, Q. Huang, Z. Li, S. Savarese, M. Savva, S. Song, H. Su, et al., "ShapeNet: An Information-Rich 3D Model Repository," *arXiv preprint arXiv:1512.03012*, 2015.
- [43] S. Fuhrmann, F. Langguth, and M. Goesele, "MVE- A Multi-View Reconstruction Environment," in *Eurographics Workshop on Graphics and Cultural Heritage*, 2014.
- [44] D. Eigen, C. Puhrsch, and R. Fergus, "Depth Map Prediction from a Single Image using a Multi-Scale Deep Network," *arXiv preprint arXiv:1406.2283*, 2014.
- [45] Y. Chen, C. Schmid, and C. Sminchisescu, "Self-Supervised Learning with Geometric Constraints in Monocular Video: Connecting Flow, Depth, and Camera," in *IEEE/CVF International Conference on Computer Vision*, 2019.
- [46] Y. Zou, P. Ji, Q.-H. Tran, J.-B. Huang, and M. Chandraker, "Learning Monocular Visual Odometry via Self-Supervised Long-Term Modeling," in *European Conference on Computer Vision*, 2020.
- [47] W. Wang, Y. Hu, and S. Scherer, "TartanVO: A Generalizable Learning-based VO," *arXiv preprint arXiv:2011.00359*, 2020.
- [48] A. Ranjan, V. Jampani, L. Balles, K. Kim, D. Sun, J. Wulff, and M. J. Black, "Competitive Collaboration: Joint Unsupervised Learning of Depth, Camera Motion, Optical Flow and Motion Segmentation," in *IEEE/CVF Conference on Computer Vision and Pattern Recognition*, 2019.
- [49] J. L. Schönberger and J.-M. Frahm, "Structure-from-Motion Revisited," in *IEEE/CVF Conference on Computer Vision and Pattern Recognition*, 2016.
- [50] C. Zheng, T.-J. Cham, and J. Cai, "T2Net: Synthetic-to-Realistic Translation for Solving Single-Image Depth Estimation Tasks," in *European Conference on Computer Vision*, 2018.
- [51] J. N. Kundu, P. K. Uppala, A. Pahuja, and R. V. Babu, "AdaDepth: Unsupervised Content Congruent Adaptation for Depth Estimation," in *IEEE/CVF Conference on Computer Vision and Pattern Recognition*, 2018.